ON THE POSSIBILITY OF USING UNDAMPED CORONAL LOOP OSCILLATIONS FOR PREDICTING POWERFUL SOLAR FLARES AND CMES

© 2025 A. B. Nechaeva[a, *], I. V. Zimovets[a], I. N. Sharykin[a], S. A. Anfinogentov[a,b]

[a]*Institute of Space Research, Russian Academy of Sciences, Moscow, Russia*

[b]*Institute of Solar-Terrestrial Physics, Siberian Branch, Russian Academy of Sciences, Irkutsk, Russia*

**e-mail: nechaeva.workspace@gmail.com*

Received February 28, 2025

Revised April 25, 2025

Accepted June 17, 2025

Abstract. In this paper, we consider undamped bending oscillations of solar coronal loops and investigate changes in their behavior in active regions (ARs) before powerful flares (M-, X-class), as well as in the absence of powerful flares. For this purpose, we analyzed 14 ARs with powerful flares and 14 ARs without powerful flares. For each event, images acquired in the 171 Å and 94 Å AIA/SDO channels were downloaded and analyzed in 12-second increments for the 4 h before the flare. For AOs without powerful flares, similarly long random time intervals were considered. Because the undamped oscillations have very low amplitude (1-2 pixels AIA/SDO), we used the Motion Magnification technique to amplify the amplitude of these oscillations. Time-distance plots were constructed from the processed images in the 171 Å channel, from which oscillatory patterns were "manually" extracted. Wavelet analysis was performed to verify the presence of changes in the oscillation period. No systematic changes were found. Also, no obvious differences in the behavior of oscillations in ARs with and without flashes were detected. Additionally, we obtained information on coronal mass ejections (CMEs) from ARs in the vicinity of the considered time intervals. Based on the results of analyzing a small sample of events, we come to the preliminary conclusion that the registration and analysis of undamped oscillations of high (~100-600 Mm) coronal loops based on this technique are unpromising for the prediction of powerful flares and CMEs.

Keywords: *Sun, active regions, coronal loops, oscillations, flares*

DOI: 10.31857/S00167940250720e1

1. INTRODUCTION

A solar flare is a process of sudden, rapid (~1-100 min) release of magnetic energy characterized by brightness enhancement across a broad spectrum of electromagnetic radiation and

observed in active regions (ARs) of the Sun [e.g., Benz, 2017]. Short-term flare prediction is an important application challenge facing solar physics. Solar flares are observed to have precursors. Precursors are, in a broad sense, a set of diverse phenomena in the AR before the (~1-2 h) of the main flare [Martin, 1980; Wang et al., 2017]. They can manifest themselves as relatively weak short (seconds-minutes) bursts of radiation intensity from localized regions of the AR, as well as in the form of amplified oscillations or fluctuations in the X-ray and radio emission bands [Kobrin et al., 1973; Zhdanov and Charikov, 1985; Chifor et al., 2007; Abramov-Maximov and Bakunina, 2020]. Apparently, the appearance of precursors is somehow related to the dynamics of magnetic fields and plasma in the AR during its evolution from a relatively quiescent state to a flare state [Priest and Forbes, 2002; Wang et al., 2017; Toriumi and Wang, 2019]. However, the mechanisms of precursors and triggers of solar flares have not yet been unambiguously established, which hinders the construction of quantitative, physically-based prediction methods.

Coronal loops are one of the main structures of ARs. It is known from observations that coronal loops can experience oscillations. In particular, two types of bending (kink) oscillations are known: damped [Nakariakov et al., 1999; White and Verwichte, 2012; Goddard et al., 2016] and undamped [Wang et al., 2012; Anfinogentov et al., 2013; Nisticò et al., 2013]. The main features of the non-damped mode are that the oscillations do not have a systematic trend of oscillation amplitude decrease, it remains practically constant (with small variations) for a long time of the order of several hours. Undamped oscillations are ubiquitous in ARs and occur even in the absence of solar flares, eruptions, or other impulsive energy releases, in contrast to damped oscillations. The periods of such oscillations are a few minutes and the amplitudes are on the order of a few Mm or less. Although the excitation mechanism of undamped oscillations is still unclear [Nakariakov et al., 2016; Karampelas and Van Doorsselaere, 2020; Afanasyev et al., 2020], the period of undamped oscillations is linearly correlated with the loop length, and hence the oscillations are natural modes of the loop [Anfinogentov et al., 2015]. An overview of the full spectrum of bending oscillations can be found in [Nakariakov et al., 2021]. The oscillations of solar coronal loops can be described in terms of the oscillations of a plasma cylinder in a magnetic field [Zajtsev and Stepanov, 1975; Roberts et al., 1984]. The period of the first harmonic (or main period) of the bending oscillations of a plasma cylinder is expressed through the loop length and bending velocity as follows:

$$P = \frac{2L}{C_K} \tag{1}$$

Here L is the loop length, and the bending velocity $C_K = c_{Ai}\left(\frac{2\xi}{\xi+1}\right)^{\frac{1}{2}}$, where ξ is the ratio of plasma densities outside and inside the loop, and the Alfvenov velocity c_{Ai} in turn depends on the plasma density in the loop and the magnetic field. Based on this, it can be assumed that during the

evolution of the parent AR, the period of the bending oscillations of the loops can change due to the rearrangement of the magnetic field and plasma characteristics. The advantage of studying undamped oscillations of coronal loops in the context of flare precursors and the possibility of their prediction is that undamped oscillations, first, can be detected in many, if not all, coronal loops [Anfinogentov et al., 2015], and second, they can be observed for hours, i.e., on the time scales of AR preparation for flares. It is also very important that they are often clearly visible near the limb, where it is difficult to observe sunspots and measure magnetic fields on the photosphere and extrapolate them to the corona, which is used to build flare forecasts [Bobra & Couvidat, 2015; Aschwanden, 2020; Zimovets & Sharykin, 2024]. Thus, our hypothesis is that in preparation of ARs for a powerful flare, the undamped coronal loop oscillations may exhibit certain patterns in their evolution that could be attempted to be used for forecasting, i.e., serve as precursors of this flare.

To test this hypothesis, as a first step, we studied 14 ARs near the solar limb in which powerful M- and X-class flares had occurred, as well as, for comparison, 14 ARs without powerful flares. For each AO, images were constructed using the Atmospheric Imaging Assembly (AIA) instrument on board the Solar Dynamics Observatory (SDO) [Lemen et al., 2012] in the 171 Å (T ~0.6 MK) and 94 Å (T ~6 MK) channels. The time step is 12 s. The behavior of the loops in ARs was studied for time intervals of 4 h preceding the flare, or for arbitrary time intervals of similar duration for ARs without powerful flares. We do not consider longer intervals because of the difficulty in applying the methodology used. In the following, we describe the methodology and the results of its application to analyze the undamped coronal loop oscillations in the considered solar ARs.

2. DATA ANALYSIS TECHNIQUE

Fourteen flares that occurred at the solar limb were selected to study the behavior of undamped bending oscillations. The criteria for selecting the flares were as follows: first, the AOs should have strong flares (above the M1.0 class), second, coronal loops should be observed in the region, and third, AOs near the limb (above 70 degrees longitude) were selected so that the loops would be observed with high contrast against the background of dark sky. A list of flashes selected for analysis, with their position and class, is given in Table 1. In two cases, in addition to the class X flare, there was also a class M flare present shortly before its onset; it is also included in the time interval considered (flashes SOL2024-06-10T11:03 X1.6 and SOL2023-08-07-07T20:30 X1.5), which is also reflected in Table 1. The table also summarizes the coronal mass ejection (CME) parameters associated with some of the considered flares, such as ST (start time), PA (position angle), AW (angular width), and LS (linear speed) from the CACTus [Robbrecht and Berghmans, 2004] and SOHO/LASCO CME Catalog (https://cdaw.gsfc.nasa.gov/CME_list/) [Gopalswamy et al., 2024]. The selection of associated CMEs was based on time (CME onset no later than an hour

and a half after the outbreak) and positional angle.

As already mentioned, AIA/SDO data in the 171 Å and 94 Å channels for 4 h before the flare in 12-second increments were used for the analysis. AO images were downloaded for each flare, in the 94 Å channel to plot the change in the integrated intensity of the hot plasma and track the change in AO, and in the 171 Å channel to further study the behavior of loops, since loops are best observed in this channel. Since the undamped oscillations have amplitudes on the order of the pixel size of the AIA/SDO instrument [Nisticò et al., 2013], to study them, the Motion Magnification algorithm [Anfinogentov and Nakariakov, 2016; Anfinogentov et al., 2019] was applied to the acquired AO images to amplify and better detect the oscillations. The algorithm uses dual tree complex wavelet transform (DTCWT) to amplify the amplitude of oscillatory processes whose temporal order is lower than w with a factor k. In this paper, we use this algorithm with amplification factor k = 5 and w = 80 frames (16 minutes). Next, time-distance diagrams are constructed for the already enhanced AO images using PyQtGraph (www.pyqtgraph.org). The slices for plotting were selected manually based on the extent to which the presence of an oscillatory pattern is visually discernible in them for further analysis. The time-distance diagrams are a demonstration of the evolution of the plasma UUV intensity in a selected slice. Figure 1a shows an example of a time-distance diagram for the SOL2023-08-07T20:30 flare. The AO in the 171 Å channel is shown on the top right, the yellow circle shows the approximate position of the flare, and the approximate area affected by the flare perturbation visible in the analyzed AIA channels is shaded in yellow, and the slice selected for analysis is shown in red. Fig. 1b shows another slice from the same AIA for the same flare. Next, the observed oscillations are manually extracted from the time-distance diagrams. The points extracted at this step are shown in blue in Fig. 1a and b. Typically, points are highlighted at the loop boundary where the contrast between the bright loop and the black background is greatest, allowing for good tracking of the oscillation pattern. Since the oscillations were manually extracted and the points lie heterogeneously on the time grid, the obtained points were approximated with a smoothing spline and additionally the spurious steppe trend was subtracted. A wavelet analysis of the observed oscillations was performed on the data points taken from this curve. The resulting wavelet spectrograms for the full 4 h before the flare are shown in Fig. 1a and b on the bottom left with the cone of influence where edge effects are strong (in translucent white), the black curve plotted with the 94 Å channel emission intensity profile. The dark gray contour indicates the 95% significance level. Separately, the 94 Å profile is also shown on the bottom right, where the vertical dashed line indicates the time of the main strong flare, and the solid vertical gray lines indicate the onset times of weaker flares in this AO during the time the region was considered. Similar results for the two AO slices where the SOL2023-01-09T18:37 flare occurred are shown in Fig. 2. It is worth noting that the spectrogram does not show

the frequency, but the product of the frequency by the loop length estimate, since this quantity is directly proportional to the bending velocity according to (1). The loop length estimate was made from the assumption that the loop is a semicircle and one can measure the loop length by knowing either the distance between the two footings (diameter) or between the center point of the footings and the apex (radius). Errors arising from the projection of the loop onto the ray of vision, possible changes in the shape of the loop during the AO review process, and deviation of the loop shape from the semicircle are not considered due to their complexity. This loop length estimation process is similar to the one used in [Goddard et al., 2016; Nechaeva et al., 2019].

For comparison with undamped loop oscillations in ARs where no powerful flares (above the M1.0 class) occurred, 14 regions with well-observed coronal loops in the 171 Å channel were further analyzed. The regions were selected so that they did not have flares above the M1.0 class during the interval in question and a few hours before and after it. A list of these regions with their coordinates and times of consideration is given in Table 2. Since there were no powerful flares in these AOs during the time intervals considered, there were no CMEs in most of the AOs considered, but for those cases where CMEs were present, information about them is also recorded in the table. Spectrograms similar to those described earlier for these AOs are shown in Figs. 3 and 4a.

To quantitatively formalize the results of wavelet analysis of oscillations, global oscillation spectra were also constructed, which represent the summation of wavelet spectra values over time. Examples of such spectra can be seen in the top panel of Fig. 5. Blue and red show the spectra for the two AO slices where the SOL2023-08-07T20:30 flare occurred, shown in Fig. 1. In black and green is shown the spectrum for oscillations from the same AO but for the time period 2023-08-08-08 from 16:00 to 20:00 UT, when there were no powerful flashes in the region (Fig. 4). Each curve was approximated by a Gaussian (dashed line) to find the mean value of the parameter "frequency multiplied by loop length", and these mean values $\langle \upsilon^* L \rangle$ and standard deviations are also entered in Tables 1 and 2. Also included in the Tables are the values of the estimate of the studied loop length L and the oscillation period P. The period was calculated based on the values for $\langle \upsilon\upsilon^* L \rangle$ and L. It is important to note that several values are given for each flash, since several slices through different loops were analyzed for a single AO. In cases where spectrograms for a slice were obtained but a particular peak could not be identified in the global spectrum, a dash (-) is indicated. For the global spectrum of the first slice for outbreak SOL2023-08-07T20:30 (blue curve in Fig. 5), the mean value is taken excluding the first peak in the spectrum, which we attribute to spurious periods. Also, for the third slice of AO 2023-08-08-08, whose oscillation spectrum is shown by the green curve, the mean value of $\langle \upsilon^* L \rangle$ was not estimated due to the large number of peaks, which is reflected in Table 2 with the results. To compare the mean values of the frequency multiplied by the loop

length, we plotted histograms for the cases of ARs with powerful flashes and ARs without powerful flashes; these are shown in the lower left panel of Fig. 5. Also in Fig. 5 bottom center and right panels are histograms for the estimated loop lengths and periods of undamped oscillations, respectively.

3. RESULTS AND CONCLUSIONS

When considering the evolution of the undamped oscillations of 35 solar coronal loops during 4 h to 14 powerful (M- and X-class) flares, no systematic changes in their behavior over the period of consideration were observed. In some individual cases, inhomogeneities in the oscillation behavior (e.g., the appearance of new frequencies or enhancement of existing ones) can be observed in wavelet spectrograms, but no clear patterns in the appearance of these inhomogeneities were detected in this sample. These inhomogeneities may be either related to physical manifestations of precursors in ARs (such as small flare events, mini-eruptions, and jets) or they may be artifacts. This issue requires further investigation. In this paper, we considered the evolution of the parameter "frequency multiplied by wavelength", i.e., the bending velocity of oscillations with a constant accuracy according to formula (1). The evolution of other oscillation parameters was not considered, and perhaps it is also of interest for further studies. The comparison found no remarkable differences in the behavior of the loop oscillations before powerful flares, and in their absence. The average frequency multiplied by the loop length is also not different for the AO cases with and without powerful flashes, as can be seen from the histograms in Fig. 5. The oscillation periods vary from a few minutes to about 20 minutes, but for large values of the periods, the errors in their determination are also large. The values of the periods obtained by a rather rough estimation from the global spectra (Fig. 5) coincide with those given in [Anfinogentov et al., 2013 and Anfinogentov et al., 2015]. Thus, we can make a preliminary conclusion that the preflare evolution of ARs does not significantly affect the bending velocity in the large (with loop lengths ~100-600 Mm) loops considered, which depends on the magnitude of the magnetic field in the loop, the plasma concentration, and the ratio of plasma densities inside and outside the loop. However, lower loops, which may be more sensitive to the magnetic field rearrangement in the AO, were not investigated in this work. In this work, we have used data from the AIA/SDO instrument, whose resolution is poor for highlighting low loops (with lengths less than 30 Mm), but there are a number of papers [Shrivastav et al., 2024; Shrivastav et al., 2025] that study undamped oscillations in low loops using data from the Extreme Ultraviolet Imager (EUI)/Solar Orbiter instrument, which has higher spatial and temporal resolution (~210 km/pixel at perihelion and 5 seconds). In the future, it may be of interest to study the undamped oscillations of relatively lower loops, which could possibly respond more strongly to changes in the magnetic field and plasma concentration in the pre-explosion phase of AO evolution.

In addition to considering the relation of undamped oscillations to flares, we also studied the relation to the presence of CMEs. For the considered ARs with powerful flares, the CME was associated with the considered events in 12 out of 14 cases (86%), and in the case without flares - in 4 out of 14 cases (29%). We also note that the 4 CMEs found for the no-flare case could be associated either with small C-class flares in the considered ARs or not at all, i.e., they could have occurred in other ARs. Since we found no obvious differences in the behavior of undamped loop oscillations in the 14 ARs with powerful flares and 14 ARs without powerful flares, we can make a preliminary conclusion that undamped oscillations of high (~100-600 Mm) loops practically do not "react" to the preparation of ARs for the realization of CME, as well as powerful flares.

It is important to note that the data analysis technique used in this work is not rigorous because the sample of ARs for analysis is small (a total of 35 slices were analyzed for the situation when a powerful flare occurred in the region and 32 slices for the situation when there was no flare), and a maximum of four slices were considered in each AR because of the quality of the raw data, since we use data in one narrow channel (171 Å). In some cases, it is not possible to track oscillations on large time scales due to changes in the temperature of the loops, whereby the loops become "invisible" to our chosen channel, but do not cease to exist. This problem can be solved by building telescopes that observe solar loops with high angular resolution (~0.1" or higher) simultaneously over a wider temperature range, and considering these data together. There are also limitations imposed by manually selecting the oscillation in the time-distance plots for analysis, and visually comparing the resulting wavelet spectrograms without using any rigorous statistical methods. Nevertheless, to the best of our knowledge, this work is the first and original attempt to use undamped coronal loop oscillations for predicting powerful solar flares and CMEs, and therefore it may be of interest as a seeded exploratory study.

ACKNOWLEDGEMENTS

We thank the SDO/AIA instrument team for free access to the data, without which this work could not have been realized. The SOHO/LASCO CME catalog is generated and maintained at the CDAW Data Center by NASA and The Catholic University of America in cooperation with the Naval Research Laboratory. SOHO is a project of international cooperation between ESA and NASA. We thank the reviewers for their helpful comments.

FUNDING

This work was supported by a grant from the Russian Science Foundation (Project No. 20-72-10158).

CONFLICT OF INTERESTS

The authors declare that they have no conflicts of interest.

REFERENCES

1. *Zhdanov A.A., Charikov Yu.E.* Frequency analysis of the pre-flare X-ray radiation of the Sun // Letters in Astron. Zh., V. 11, P. 216-221, 1985.
2. *Abramov-Maximov V.E. and Bakunina I.A.* Oscillations of the Microwave Emission of Solar Active Region 12673 before Flares // Geomagnetism and Aeronomy, V. 59, N. 7, P. 822–826, 2020. doi:10.1134/S001679321907003X.
3. *Afanasyev A.N., Van Doorsselaere T., and Nakariakov V.M.* Excitation of decay-less transverse oscillations of coronal loops by random motions // A&A, V. 633, L8. 2020. doi:10.1051/0004-6361/201937187.
4. *Anfinogentov S., Nisticò G., and Nakariakov V.M.* Decay-less kink oscillations in coronal loops // A&A, V. 560, A107. 2013. doi:10.1051/0004-6361/201322094.
5. *Anfinogentov S.A., Nakariakov V.M., and Nisticò G.* Decayless low-amplitude kink oscillations: a common phenomenon in the solar corona? // A&A, V. 583, A136, 2015. doi:10.1051/0004-6361/201526195.
6. *Anfinogentov S. and Nakariakov V.M.* Motion Magnification in Coronal Seismology // SoPh, V. 291, N. 11, P. 3251–3267, 2016. doi:10.1007/s11207-016-1013-z.
7. *Anfinogentov S., Nakariakov V., Kosak K.* DTCWT based motion magnification v0.5.0 // Zenodo. 2019.
8. *Aschwanden M.J.* Global Energetics of Solar Flares. XI. Flare Magnitude Predictions of the GOES Class // ApJ, V. 897, N. 1, 16, 2020. doi:10.3847/1538-4357/ab9630.
9. *Benz A.O.* Flare Observations // Living Reviews in Solar Physics, V. 14, N. 1, 2, 2017. doi:10.1007/s41116-016-0004-3.
10. *Bobra, M.G. and Couvidat S.* Solar Flare Prediction Using SDO/HMI Vector Magnetic Field Data with a Machine-learning Algorithm // ApJ, V. 798, N. 2, 135, 2015. doi:10.1088/0004-637X/798/2/135.
11. *Chifor C., Tripathi D., Mason H.E., Dennis B.R.* X-ray precursors to flares and filament eruptions // Astron. & Astrophys., V. 472. P. 967-979. 2007. doi:10.1051/0004-6361:20077771.
12. *Goddard C.R., Nisticò G., Nakariakov V.M. et al.* A statistical study of decaying kink oscillations detected using SDO/AIA" // A&A, V. 585, A137, 2016. doi:10.1051/0004-6361/201527341.
13. *Gopalswamy N., Michałek G., Yashiro S. et al.* The SOHO LASCO CME Catalog – Version 2 // arXiv e-prints. arXiv:2407.04165. 2024. doi:10.48550/arXiv.2407.04165.
14. *Karampelas K. and Van Doorsselaere T.* Generating Transverse Loop Oscillations through a Steady-flow Driver // ApJ, V. 897, N. 2, L35, 2020. doi:10.3847/2041-8213/ab9f38.

15. *Kobrin M.M., Korshunov A.I., Snegirev S.D., Timofeev B.V.* On a sharp increase of quasi-periodic components of fluctuations of inclination of the spectrum of solar radio emission at lambda = 3 cm before active events in August 1972 // Soln. Dannye, V. 10, P. 79-85, 1973.
16. *Lemen J.R., Title A.M., Akin D.J. et al.* The Atmospheric Imaging Assembly (AIA) on the Solar Dynamics Observatory (SDO) // SoPh, V. 275, N. 1–2, P. 17–40, 2012. doi:10.1007/s11207-011-9776-8.
17. *Martin S.F.* Preflare conditions, changes and events // SoPh, V. 68, N. 2, P. 217–236, 1980. doi:10.1007/BF00156861.
18. *Nakariakov V.M., Ofman L., Deluca E.E. et al.* TRACE observation of damped coronal loop oscillations: Implications for coronal heating // Science, V. 285, P. 862–864. 1999, doi:10.1126/science.285.5429.862.
19. *Nakariakov V.M., Anfinogentov S.A., Nisticò G. et al.* Undamped transverse oscillations of coronal loops as a self-oscillatory process // A&A, V. 591, L5, 2016. doi:10.1051/0004-6361/201628850.
20. *Nakariakov V.M., Anfinogentov S.A., Antolin, P. et al.* Kink Oscillations of Coronal Loops // Space Sci Rev V. 217, N. 73, 2021. https://doi.org/10.1007/s11214-021-00847-2.
21. *Nechaeva A., Zimovets I.V., Nakariakov V.M., et al.* Catalog of Decaying Kink Oscillations of Coronal Loops in the 24th Solar Cycle // ApJS, V. 241, N. 2, 31, 2019. doi:10.3847/1538-4365/ab0e86.
22. *Nisticò G., Nakariakov V.M., Verwichte E.* Decaying and decayless transverse oscillations of a coronal loop // A&A, V. 552, A57, 2013. doi:10.1051/0004-6361/201220676.
23. *Priest E.R. and Forbes T.G.* The magnetic nature of solar flares // Astronomy and Astrophysics Review, V. 10, N. 4, P. 313–377, 2002. doi:10.1007/s001590100013.
24. *Roberts B., Edwin P.M., and Benz A.O.* On coronal oscillations // ApJ, V. 279, P. 857–865, 1984. doi:10.1086/161956.
25. *Robbrecht E. and Berghmans D.* Automated recognition of coronal mass ejections (CMEs) in near-real-time data // A&A, V. 425, P. 1097–1106, 2004. doi:10.1051/0004-6361:20041302.
26. *Shrivastav A.K., Pant V., Berghmans D. et al.* Statistical investigation of decayless oscillations in small-scale coronal loops observed by Solar Orbiter/EUI // A&A, V. 685, A36, 2024. doi:10.1051/0004-6361/202346670.
27. *Shrivastav A.K., Pant V., Berghmans D. et al.* On the Existence of Long-period Decayless Oscillations in Short Active Region Loops // ApJ, V. 979, N. 1, A6, 2025. doi:10.3847/1538-4357/ad95fb.
28. *Toriumi S., Wang H.* Flare-productive active regions // Living Rev Sol. Phys., V. 16, N. 3,

2019. https://doi.org/10.1007/s41116-019-0019-7.

29. *Wang H., Liu C., Ahn K. et al.* High-resolution observations of flare precursors in the low solar atmosphere // Nature Astronomy, V. 1, 0085, 2017. doi:10.1038/s41550-017-0085.
30. *Wang T., Ofman L., Davila J.M., et al.* Growing Transverse Oscillations of a Multistranded Loop Observed by SDO/AIA // ApJ, V. 751, N. 2, L27, 2012. doi:10.1088/2041-8205/751/2/L27.
31. *White, R.S. and Verwichte, E.* Transverse coronal loop oscillations seen in unprecedented detail by AIA/SDO // A&A, V. 537, A49, 2012. doi:10.1051/0004-6361/201118093.
32. *Zajtsev V.V. and Stepanov A.V.* On the origin of pulsations of type IV solar radio emission. Plasma cylinder oscillations (I) // Issledovaniia Geomagnetizmu Aeronomii i Fizike Solntsa, V. 37, P. 3–10, 1975.
33. *Zimovets I.V. and Sharykin I.N.* Models for Short-Term Forecast of Maximum X-ray Class of Solar Flares Based on Magnetic Energy of Active Regions // Geomagnetism and Aeronomy, V. 64, N. 5, P. 603–61, 2024. doi:10.1134/S0016793224600541.
34. https://cdaw.gsfc.nasa.gov/CME_list/
35. www.pyqtgraph.org

Table 1. List of flares used for the analysis of undamped oscillations 4 hours before the flare, with their position and class, and associated coronal mass ejections with the parameters: start time (ST - start time), position angle (PA - position angle), angular width (AW - angular width), and velocity (LS - linear speed) from the CACTus and SOHO/LASCO CME Catalogs. The last column shows the mean value of the frequency multiplied by the loop length ⟨υ*L⟩ obtained from the global spectrum, as well as the loop length L and the oscillation period P for each analyzed slice.

Flash	**GOES Class // AO position (heliographic coordinates)**	**CME**	**⟨υ*L⟩, [Hz*Mm]** **L, [Mm]** **P, [min]**
SOL2024-08-14T03:33	M4.4 // S03W89	ST 24/08/14 04:12 PA 276° (AW 212°) LS 546 km/sec.	1.19 ± 0.43 336 4.71 ± 1.70
			2.68 ± 1.21 654 4.07 ± 1.83
SOL2024-07-16T13:11	X1.9 // S05W83	ST 24/07/16 13:48 PA 277° (AW 92°) LS 520 ± 210 km/sec.	0.33 ± 0.15 80 4.04 ± 1.84
			0.34 ± 0.29 116 5.69 ± 4.85
			- 85 -
SOL2024-06-10T11:03 SOL2024-06-10T10:18	X1.6 // S17W89 M5.3 // S17W89	ST 24/06/10 10:48 PA 284° (AW 246°) LS 972 km/sec.	0.83 ± 0.43 398 7.99 ± 4.14
			1.10 ± 0.32 450

			6.82 ± 1.98
			0.81 ± 0.56 367 7.55 ± 5.22
SOL2024-05-27T06:49	X2.9 // S18E89	ST 24/05/27 07:12 PA 75° (AW 228°) LS 762 ± 319 km/sec	1.39 ± 0.49 596 7.15 ± 2.52
			1.89 ± 0.89 574 5.06 ± 2.38
SOL2024-05-15T14:20	X3.0 // S12E89	-	1.89 ± 0.68 610 5.38 ± 1.94
			1.82 ± 0.41 498 4.56 ± 1.02
			1.83 ± 0.34 498 4.53 ± 0.84
SOL2024-05-15T08:15	X3.5 // S18W89	ST 24/05/15 08:48 PA 144° (AW 360°) LS 1250 ± 685 km/sec.	- 671 -
			1.37 ± 0.87 733 8.92 ± 5.66

SOL2024-05-14T16:46	X8.7 // S18W89	ST 24/05/14 16:48 PA 244° (AW 34°) LS 1037 ± 451 km/sec	1.14 ± 0.69 665 9.72 ± 5.79
			0.86 ± 0.55 629 12.19 ± 7.80
SOL2024-05-14T12:40	X1.2 // S17W89	ST 24/05/14 13:00 PA 266° (AW 78°) LS 749 km/sec.	- 590 -
			0.52 ± 0.32 631 20.22 ± 12.44
			- 229 -
SOL2024-02-09T12:53	X3.4 // S37W85	ST 24/02/09 13:25 PA 158° (AW 138°) LS 992 ± 340 km/sec.	1.19 ± 0.67 793 11.11 ± 6.25
			1.85 ± 1.61 635 5.72 ± 4.98
			- 673 -
SOL2023-08-07T20:30 SOL2023-08-07T19:37	X1.5 // N12W88 M1.4 // N19W75	ST 23/08/07 20:36 PA 340° (AW 42°) LS 416 ± 659 km/sec	0.37 ± 0.15 359 16.17 ± 6.56
			0.60 ± 0.11 274

			7.61 ± 1.39
			0.45 ± 0.50 298 11.04 ± 12.26
SOL2023-06-20T16:42	X1.1 // S17E73	ST 23/06/20 17:12 PA 87° (AW 108°) LS 679 ± 81 km/sec.	0.51 ± 0.53 207 6.76 ± 7.03
SOL2023-01-09T18:37	X1.9 // S13E71	ST 23/01/09 19:12 PA 73° (AW 8°) LS 618 ± 225 km/sec.	0.80 ± 0.24 199 4.14 ± 1.24
		PA 46° (AW 14°) LS 857 ± 87 km/sec	0.75 ± 0.41 301 6.69 ± 3.66
			0.89 ± 0.60 226 4.23 ± 2.85
SOL2023-01-06T00:43	X1.2 // S20E81	-	- 261 -
SOL2022-04-30T13:37	X1.1 // N15W100	ST 22/04/30 14:00 PA 260° (AW 187°) LS 498 km/sec.	0.65 ± 0.10 149 3.82 ± 0.58
			- 485 -
			1.19 ± 0.83 564 7.90 ± 5.51

			1.26 ± 0.32 536 7.09 ± 1.80

Table 2. Active regions used to analyze the undamped oscillations in the absence of powerful flares, the time interval at which they were considered, and their position. The last column shows the mean value of the frequency multiplied by the loop length ⟨υ*L⟩ obtained from the global spectrum, as well as the loop length L and the oscillation period P for each slice analyzed.

Date and time interval UT	**AO position (heliographic coordinates)**	**CMC**	**⟨υ*L⟩, [Hz*Mm] L, [Mm] P, [min]**
2024-08-28 04:00-08:00	S14E88	-	0.53 ± 0.17 232 7.29 ± 2.34
			0.89 ± 0.43 339 6.35 ± 3.07
			2.16 ± 0.63 601 4.64 ± 1.35
2024-07-18 04:00-08:00	S9W86	ST 24/07/18 07:24 PA 120° (AW 42°) LS 441 km/sec.	1.44 ± 0.66 586 6.78 ± 3.11
			- 612 -
2024-06-11 08:00-12:00	S13E86	-	1.21 ± 0.38 301 4.15 ± 1.40
			1.35 ± 0.52 354 4.37 ± 1.68

			1.24 ± 1.06 554 7.45 ± 6.37
2024-05-19 04:00-08:00	N21W89	-	1.12 ± 0.54 366 5.45 ± 2.62
			1.34 ± 1.40 523 6.50 ± 6.79
2023-08-08 16:00 - 20:00	N12W88	-	0.58 ± 0.28 230 6.61 ± 3.19
			0.82 ± 0.20 266 5.41 ± 1.32
			- 104 -
2023-07-20 08:00 - 12:00	S25W85	ST 23/07/20 09:48 PA 254° (AW 28°) LS 672 km/sec.	1.55 ± 0.88 647 6.96 ± 3.95
			1.51 ± 0.42 496 5.47 ± 1.52
2023-06-21 00:00 - 04:00	N17E73	-	- 226 -
			0.54 ± 0.21 163

			5.03 ± 1.96
2023-04-07 08:00 - 12:00	N11W87	-	0.82 ± 0.24 220 4.47 ± 1.31
			1.42 ± 0.48 399 4.68 ± 1.58
			1.16 ± 0.89 397 5.70 ± 4.38
2023-04-01 16:00 - 20:00	S22W84	-	1.64 ± 0.83 621 6.31 ± 3.19
			1.12 ± 0.85 390 5.80 ± 4.40
			- 345 -
			0.69 ± 0.47 308 7.43 ± 5.06
			0.78 ± 0.21 416 8.89 ± 2.39
2023-01-10 08:00 - 12:00	S13E69	ST 23/01/10 13:25 PA 75° (AW 32°) LS 473 km/sec.	0.50 ± 0.27 162 5.40 ± 2.91
2023-01-07	S13E80	-	0.26 ± 0.10

08:00 - 12:00			254 16.28 ± 6.26
2022-12-28 08:00 - 12:00	S19E87	-	1.76 ± 0.82 612 5.79 ± 2.70
			1.21 ± 0.25 303 4.17 ± 0.86
2022-12-18 08:00 - 12:00	N25E88	-	1.01 ± 0.43 391 6.45 ± 2.75
2022-05-01 08:00 - 12:00	N15W91	ST 22/05/01 08:36 PA 251° (AW 240°) LS 700 km/sec.	0.82 ± 0.26 398 8.09 ± 2.56
			0.56 ± 0.41 365 10.86 ± 7.95

FIGURE CAPTIONS

Fig. 1. Results of the two slice analysis for flash SOL2023-08-07T20:30. Each of panels a) and b) shows the time-distance plots in the 171 Å channel on the top left, with manually selected blue oscillation points for analysis. The wavelet spectrogram for the "frequency times loop length" parameter is shown below, with a cone of influence where edge effects are strong (in translucent white). The black line plots the integral intensity curve of the plasma emission in the 94 Å channel from the considered AO. The top right shows the 171 Å channel image of the AO itself with the studied slice (red line). The approximate position of the flare and the cone affected by the perturbation are shown in yellow semi-transparent. The same intensity curve in the 94 Å channel is shown below, with gray vertical straight lines plotted with the onset times of the fainter flares: SOL2023-08-07-07T19:37 (M1.4).

Fig. 2. Results of the two slice analysis for the flash SOL2023-01-09T18:37, similar to those presented in Fig. 1. Fainter flashes in the region during the time of consideration are SOL2023-01-09T14:48 (C7.8), SOL2023-01-09T15:43 (C5.1), and SOL2023-01-09T16:03 (C4.1).

Fig. 3. Results of the two slice analysis for AO 2023-04-01 from 16:00 to 20:00, in which no powerful flares occurred, similar to those in Fig. 1.

Fig. 4. Results of the two slice analysis for AO 2024-08-08-08 from 16:00 to 20:00, in which no powerful flashes occurred, similar to those presented in Fig. 1. The fainter flashes in the region during the time of consideration are SOL2023-08-08-08T16:45 (C1.5), SOL2023-08-08-08T19:52 (C1.7).

Fig. 5. Integral wavelet spectra for the slices shown in Figs. 1a (blue curve) and 1b (red curve) and Fig. 4a (black curve) and 4b (green curve). The first three spectra are approximated by Gaussians (dashed lines) to find the average frequency multiplied by the loop length. The spectrum for slice 4b cannot be approximated by a Gaussians due to the large number of peaks in it, which is reflected in the table (see Table 2 for 2024-08-08-08 slice 3). The bottom left panels show histograms for the average frequency times the loop length estimated from the integrated spectra, in blue for ARs with powerful flares, and in red for ARs without powerful flares. Similarly, the bottom panels at the center and right show histograms for the estimated length of the considered loops and the oscillation period, respectively.

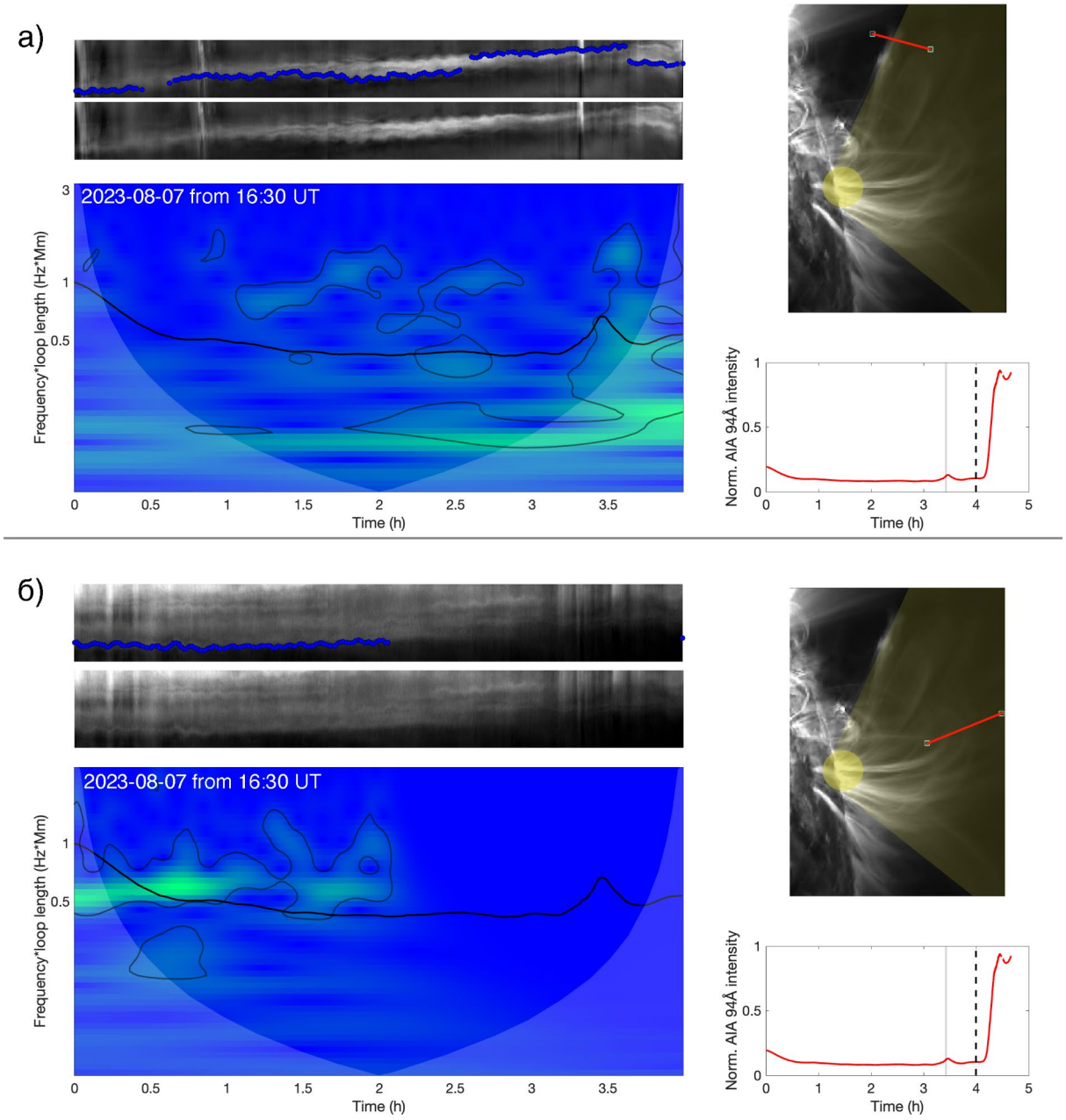
а)
2023-08-07 from 16:30 UT
Frequency*loop length (Hz*Mm)
Time (h)
Norm. AIA 94Å intensity
Time (h)
б)
2023-08-07 from 16:30 UT
Frequency*loop length (Hz*Mm)
Time (h)
Norm. AIA 94Å intensity
Time (h)

Fig. 1.

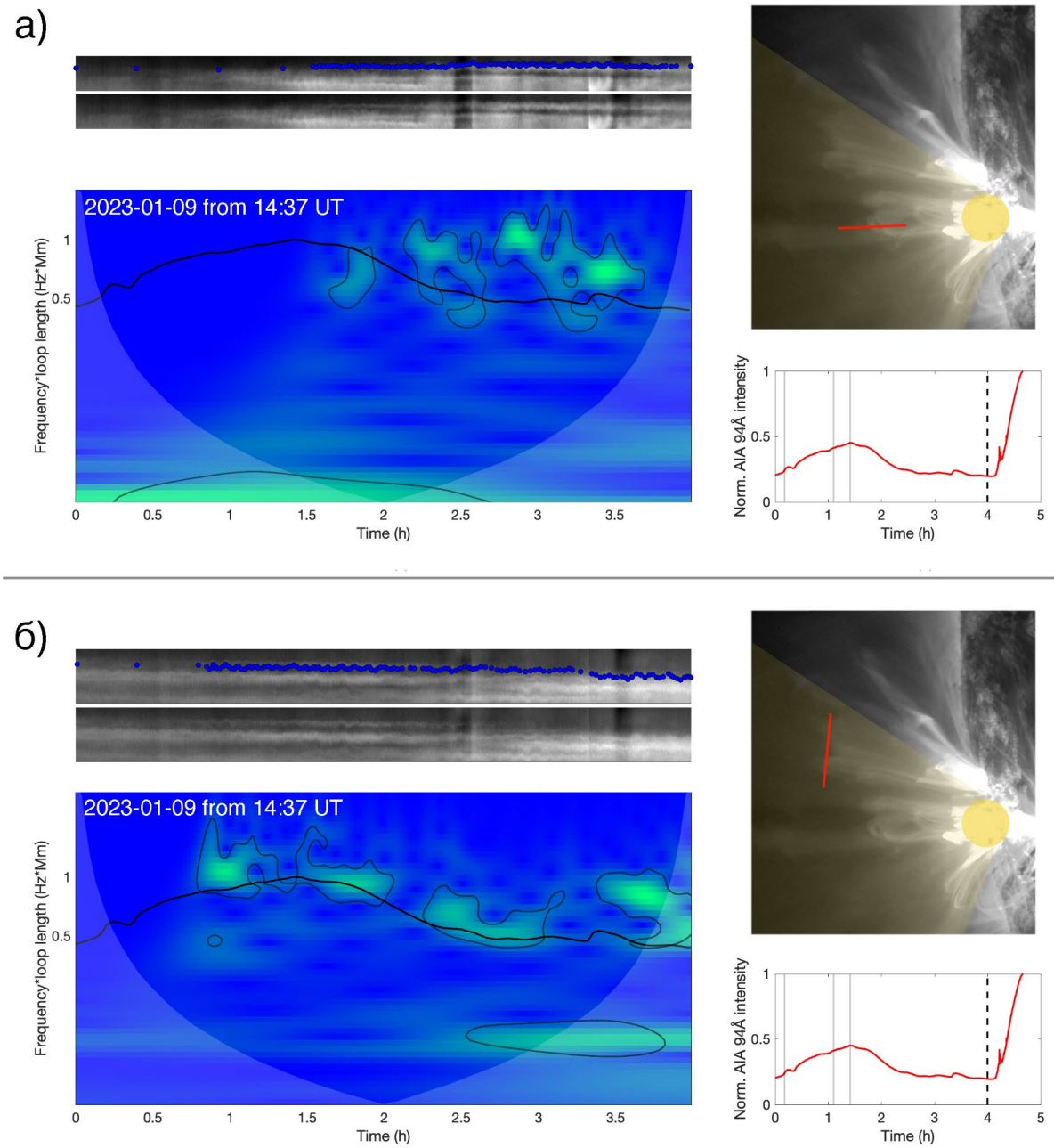
а)
2023-01-09 from 14:37 UT
Frequency*loop length (Hz*Mm)
Time (h)
Norm. AIA 94Å intensity
Time (h)
б)
2023-01-09 from 14:37 UT
Frequency*loop length (Hz*Mm)
Time (h)
Norm. AIA 94Å intensity
Time (h)

Fig. 2.

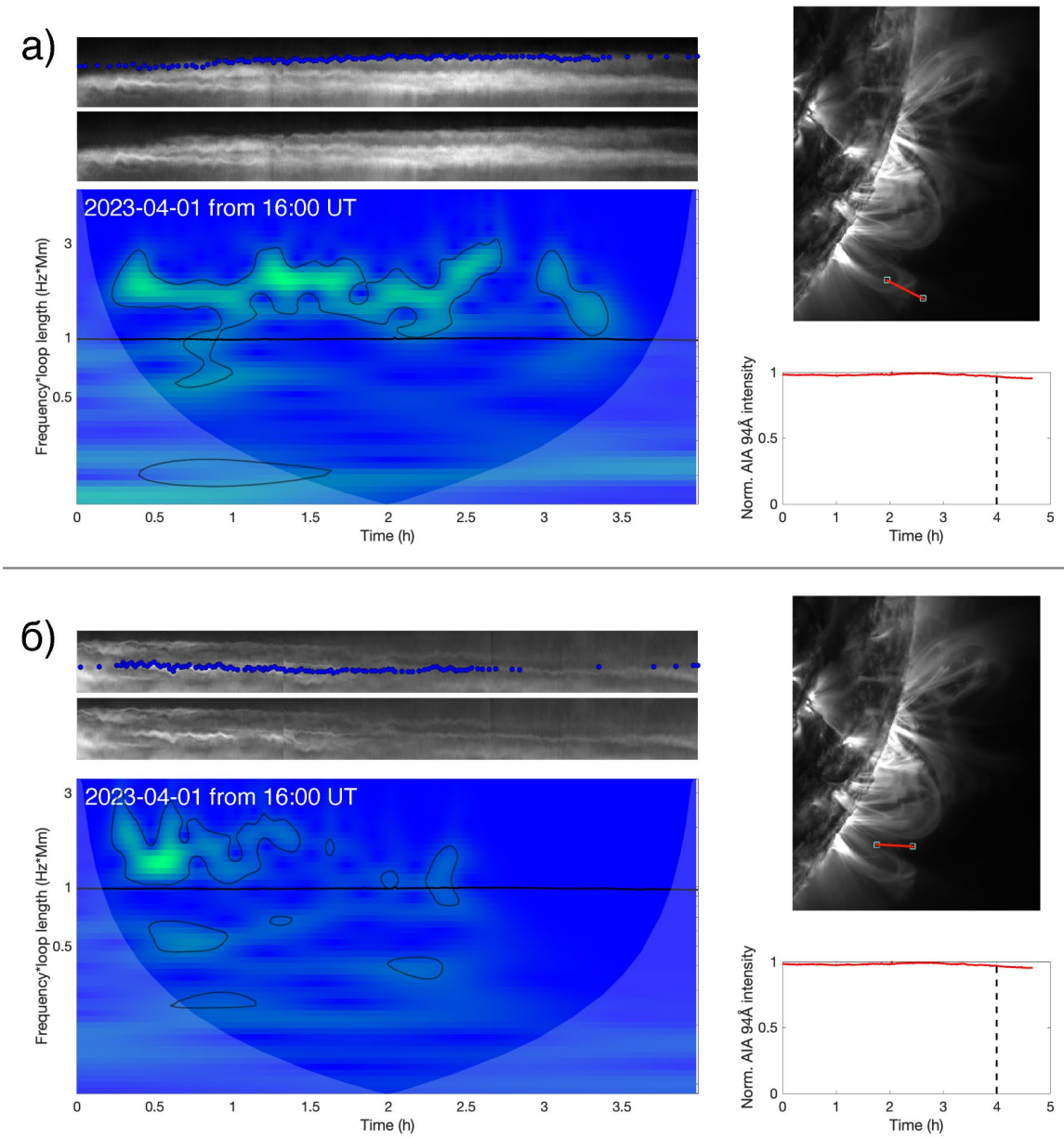
а)
2023-04-01 from 16:00 UT
Frequency*loop length (Hz*Mm)
Time (h)
Norm. AIA 94Å intensity
Time (h)
б)
2023-04-01 from 16:00 UT
Frequency*loop length (Hz*Mm)
Time (h)
Norm. AIA 94Å intensity
Time (h)

Fig. 3.

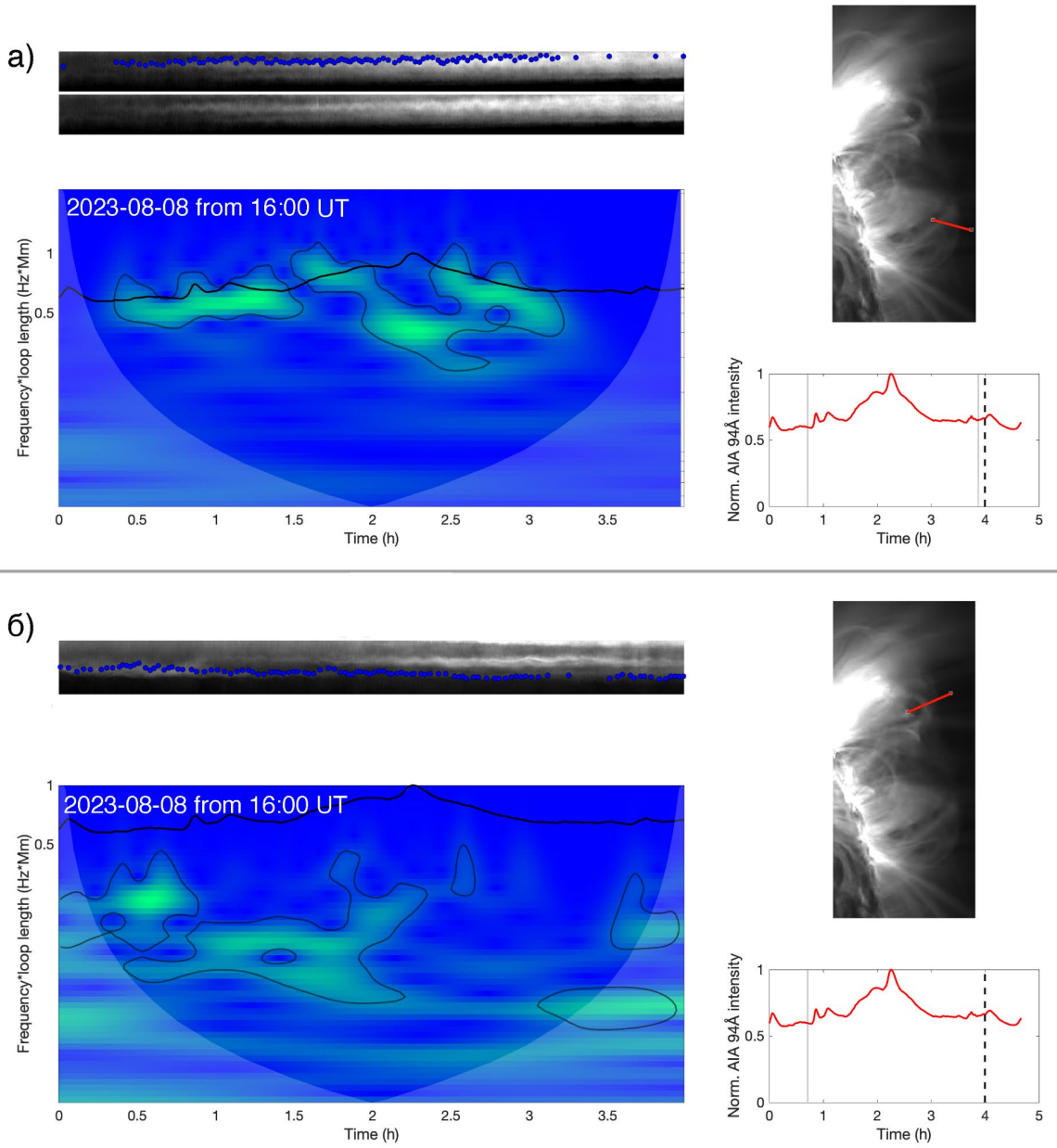
а)
2023-08-08 from 16:00 UT
Frequency*loop length (Hz*Mm)
Time (h)
Norm. AIA 94Å intensity
Time (h)
б)
2023-08-08 from 16:00 UT
Frequency*loop length (Hz*Mm)
Time (h)
Norm. AIA 94Å intensity
Time (h)

Fig. 4.

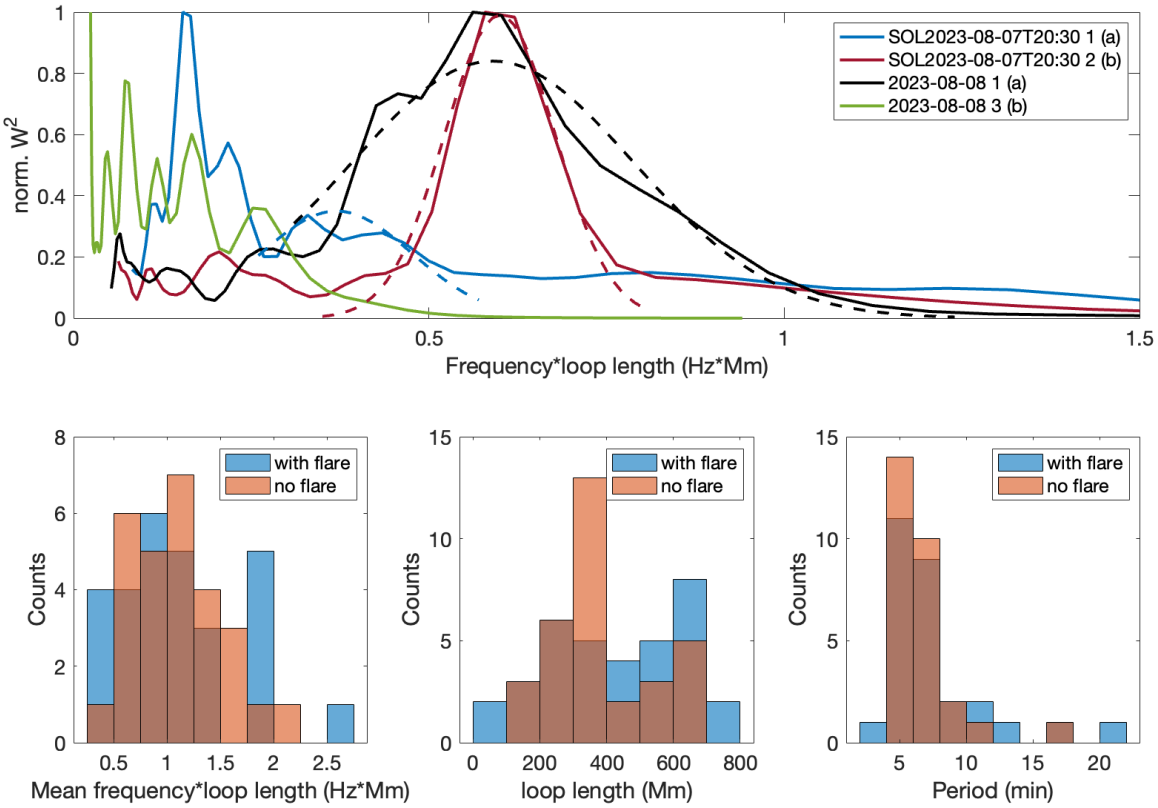
SOL2023-08-07T20:30 1 (a)
SOL2023-08-07T20:30 2 (b)
2023-08-08 1 (a)
2023-08-08 3 (b)
norm. W^2
Frequency*loop length (Hz*Mm)
with flare
no flare
Counts
Mean frequency*loop length (Hz*Mm)
loop length (Mm)
Period (min)

Fig. 5.